

Manuscript version: Author's Accepted Manuscript

The version presented in WRAP is the author's accepted manuscript and may differ from the published version or Version of Record.

Persistent WRAP URL:

<http://wrap.warwick.ac.uk/118365>

How to cite:

Please refer to published version for the most recent bibliographic citation information. If a published version is known of, the repository item page linked to above, will contain details on accessing it.

Copyright and reuse:

The Warwick Research Archive Portal (WRAP) makes this work by researchers of the University of Warwick available open access under the following conditions.

Copyright © and all moral rights to the version of the paper presented here belong to the individual author(s) and/or other copyright owners. To the extent reasonable and practicable the material made available in WRAP has been checked for eligibility before being made available.

Copies of full items can be used for personal research or study, educational, or not-for-profit purposes without prior permission or charge. Provided that the authors, title and full bibliographic details are credited, a hyperlink and/or URL is given for the original metadata page and the content is not changed in any way.

Publisher's statement:

Please refer to the repository item page, publisher's statement section, for further information.

For more information, please contact the WRAP Team at: wrap@warwick.ac.uk.

Identification of Incident Parameters of Interference Beams Using Angular Power Spectral Density

Yumeng Song, Xianping Liu, Yanling Tian*

School of Engineering, University of Warwick, Coventry, CV4 7AL, UK

Corresponding author email: y.tian.1@warwick.ac.uk

Abstract: Laser interference lithography is attracting increasing interest of researchers because of its high-efficiency and low-cost in fabrication of patterns. However, there are always operational errors in the set-up of interference systems, which have a significant effect on the final produced interference pattern. This paper has systematically investigated the influences of incident parameters including incident angle, azimuth angle and polarization angle on interference patterns. An algorithm has been proposed to extract interference fringes from complicated multi-beam interference patterns using the angular power spectral density (APSD) function. The incident parameters were calculated based on the data extracted from the APSD images. Simulations were carried out to validate the effectiveness of the proposed algorithm. 3-D periodic patterns were fabricated on silicon wafers using three-beam interference lithography. The topographies of the samples were measured using an optical profiler. Based on the established model, incident parameters of the interference system set-up were calculated. The computational results are in good agreement with the pre-set values. The results have demonstrated the validation of the developed algorithm for incident parameter identification of interference beams.

1. Introduction

Laser induced fabrication has long been used as one of the common methods to fabricate functional surfaces [1]. Among them, laser interference lithography is an efficient technique to fabricate periodic micro- and nano-structures. The fabrication speed can reach 0.9 m²/min [2, 3]. The spatial resolution of structures can be achieved for a range from 300 nm to several microns [4, 5]. Compared with another widely utilized technique, direct laser writing, which can only process structures as small as 25 μm [6], with a relative low speed of areal fabrication, depending on the structure size [2], laser interference lithography shows great superiority in structure size and processing efficiency.

With laser interference lithography, structures can be processed on large areas with multiple exposure [3]. This paved the way for numerous applications including fabrication of hydrophobic surfaces [4, 7], anti-reflective surfaces for solar cells [8-10], photonic crystals [11], micro lenses [12], substrates for growth of multi-scale structures [13, 14] and many other functional surfaces. With proper selection of different incident parameters, various patterns can be generated using laser interference lithography.

Different types of laser interference system set-ups have been established, including diffractive optical elements (DOE) induced configurations [15, 16] and beam splitter induced configurations [17, 18]. For the DOE system configurations, the parameters of different incident beams can only be adjusted simultaneously by changing optical elements. In contrast to the DOE configurations, the beam splitter induced configurations offer the flexibility in adjusting and tuning the incident parameters through individual incident beams. However, in beam splitter configurations, position errors are very common due to the manual operations in

the setting up process. A misalignment in the set-up may cause a distortion in the interference pattern [18, 19]. For periodically patterned functional surfaces, a change in the period, size, shape or depth of the structures may all affect the practical performance [20]. Hence, it is of great importance to calibrate the incident parameters in order to minimise the influence of error in the set-up of the interference system.

Efforts have been made to calibrate the incident parameters in two-beam interference systems by manually measurements of the structure period on the sample surfaces [21, 22], however, significant errors can exist in manual measurements. It is also a challenge to measure directly the complicated patterns generated by multi-beam interference. The Fast Fourier Transform (FFT) has been applied in the characterization of two-beam interference patterns [3, 23]. By extracting other information from the angular power spectral density (APSD) image, which is generated from the FFT result, it is possible to calibrate the incident parameters in multi-beam interference.

This paper analyses the generation process of the interference pattern, as well as the influences of incident angle, azimuth angle and polarization angle on the interference pattern. An algorithm is established to extract period, orientation and intensity of interference fringes from the interference pattern, and calculate the incident parameters of the laser beams with the APSD function. Simulation and experiment have been conducted to validate the established algorithm and technique. This method can be applied for interference system set-up calibration and alignment compensation.

2. Theoretical modelling

2.1 Generation of interference pattern

When laser beams with the same wavelength are incident at the same point on the sample surface from different directions, the beams interfere with each other and an interference pattern appears on the surface. It is necessary to investigate the generation of the patterns, and analyse the influence of different incident parameters, including incident angle θ , azimuth angle ϕ and polarization angle α .

The intensity of a laser beam at the point (x, y, z) in an n-beam spatial interference can be calculated by [22]

$$I \propto E^2 = \frac{1}{2} \sum_{i=1}^n a_i^2 + \frac{1}{2} \sum_{i=1}^n \sum_{j=1}^n (\mathbf{p}_i \cdot \mathbf{p}_j) a_i a_j \cos(\mathbf{k} \cdot [(\mathbf{r}_i \cdot \mathbf{d}) - (\mathbf{r}_j \cdot \mathbf{d})] + \delta_i - \delta_j) \quad (1)$$

where I is the intensity of the pattern, E is the sum of the electric fields of all the incident laser beams, a_i ($i=1, 2, \dots, n$) are the amplitudes of the electric fields of the laser beams, δ_i ($i=1, 2, \dots, n$) are the initial phases of the laser beams, $\mathbf{d} = x \cdot \mathbf{i} + y \cdot \mathbf{j} + z \cdot \mathbf{k}$ is the position vector of the point, \mathbf{r}_i ($i=1, 2, \dots, n$) are the propagation vectors and \mathbf{p}_i ($i=1, 2, \dots, n$) are the polarization vectors, which can be calculated from equations (2) and (3), respectively.

$$\mathbf{r}_i = -\sin \theta_i \cos \phi_i \cdot \mathbf{i} - \sin \theta_i \sin \phi_i \cdot \mathbf{j} - \cos \theta_i \cdot \mathbf{k} \quad (2)$$

$$\mathbf{p} = (-\cos \alpha_i \cos \phi_i \cos \theta_i - \sin \alpha_i \sin \phi_i) \cdot \mathbf{i} - (\cos \alpha_i \sin \phi_i \cos \theta_i - \sin \alpha_i \cos \phi_i) \cdot \mathbf{j} + \cos \alpha_i \sin \theta_i \cdot \mathbf{k} \quad (3)$$

2.2 Influence of incident parameters on interference pattern

The incident parameters including incident angle, azimuth angle, polarization angle and initial phase may all affect the intensity distribution of the interference fringes. It can be observed from equation (1) that the interference components in multi-beam interference is the superposition of the interference components of each pair of incident beams. By investigating the relationship between different incident parameters and the interference pattern, incident parameters can be identified backwards from the interference pattern. This will provide valuable guidance in the calibration of the interference system. The period of the interference pattern (P) can be found by [21]

$$P = \frac{\lambda}{\sqrt{(\cos \phi_1 \sin \theta_1 - \cos \phi_2 \sin \theta_2)^2 + (\sin \phi_1 \sin \theta_1 - \sin \phi_2 \sin \theta_2)^2}} \quad (4)$$

where λ is the wavelength of the laser source, ϕ_i ($i=1, 2$) and θ_i ($i=1, 2$) are the azimuth angles and incident angles of the laser beams, respectively.

The orientation of the fringes can be expressed by the azimuth angle of the pattern (γ), which can be expressed as

$$\tan \gamma = \frac{\cos \phi_1 \sin \theta_1 - \cos \phi_2 \sin \theta_2}{\sin \phi_1 \sin \theta_1 - \sin \phi_2 \sin \theta_2} \quad (5)$$

The pattern intensity is determined not only by the intensity of the laser source, but also by the polarization directions of two laser beams, which are defined as polarization vectors (\mathbf{p}), and can be calculated with equation (3). The intensity of the interference component (A) is defined as

$$A = 2a_1 a_2 (\mathbf{p}_1 \cdot \mathbf{p}_2) \quad (6)$$

3. APSD function and simulation of incident parameters calculation

As explained above, all multi-beam interference patterns can be treated as the superposition of the interference fringes of each pair of laser beams. However, since for an n-beam interference pattern the number of interference components is given by:

$$N = \frac{n(n-1)}{2} \quad \text{and the interference components}$$

overlap with each other, it is not always that straightforward to measure the period, orientation or relative intensity of each interference component.

In order to extract all the interference components, the Angular Power Spectral Density (APSD) function was introduced. Fig. 1(a) is a simulated laser intensity distribution for a 3-beam interference pattern, with the laser source wavelength $\lambda=1064$ nm and the other parameters of $\theta_1=3^\circ$, $\theta_2=4^\circ$, $\theta_3=5^\circ$, $\phi_1=0^\circ$, $\phi_2=120^\circ$, $\phi_3=240^\circ$, $\alpha_1=\alpha_2=\alpha_3=0^\circ$. Fig. 1(b) shows the corresponding APSD image, where the three peaks in the red circle represent the three interference components. To extract the information of each interference component, a circular scan was performed across the APSD image, as shown in Fig. 1(c). The maximum intensity along each orientation during the scanning process was recorded and is shown in Fig. 1(d). Then the corresponding period of each peak was read from the distance between the peak and the centre of the APSD image. A two dimensional Gaussian window was applied to each peak and the sum of the heights under the peak is recorded as the relative intensity of that interference component. An equation set can be generated using the period, orientation and relative intensity of each interference component based on equations (4)-(6). By solving the equation set, the incident parameters including the incident angle and azimuth angles of all the incident beams can be obtained.

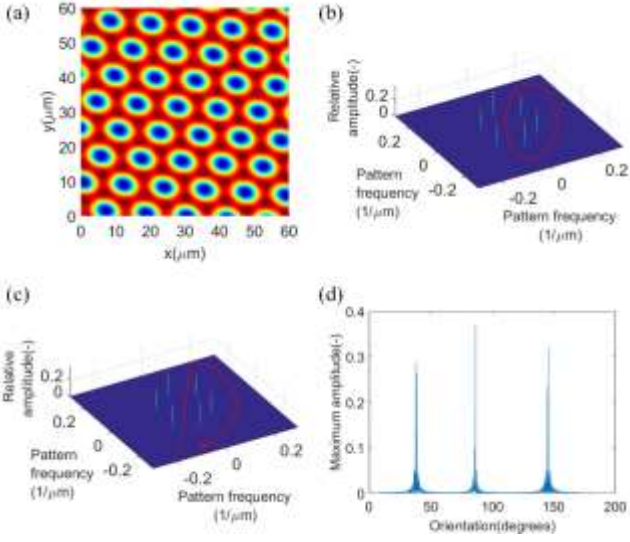


Fig. 1 A three-beam interference pattern and APSD analysis. (a) Simulated laser intensity distribution of 3-beam laser interference. (b) APSD image of the pattern in (a). (c) The scanning process of the peaks in the APSD image. (d) The orientations of the peaks in (b).

The simulations were conducted for four interference patterns, which were all generated by three-beam interference. All the polarization angles were selected to be transverse magnetic (TM). The incident parameters are listed in Table 1 and the interference patterns Nos. 1-4 are shown in Fig. 2(a)-(d).

Table 1 Incident parameters used to generate interference patterns

No.	θ_1	θ_2	θ_3	ϕ_1	ϕ_2	ϕ_3
1	5.0	5.0	5.0	0	120	240
2	7.0	2.0	6.0	0	120	240
3	5.0	5.0	5.0	10	127	235
4	5.3	7.4	3.9	308	103	24

APSD images were used to extract the interference components for all of the interference patterns, the obtained period, orientation and relative intensity of each component are listed in Table 2.

Then the incident parameters were calculated and are shown in Table 3. It can be observed that the identification of incident parameters is accurate, the error of incident angle is smaller than 0.1° and the error of azimuth angle is smaller than 1° . The results show the

Table 2 Parameters of the interference components

No.	Period ($P / \mu\text{m}$)			Orientation ($\gamma / ^\circ$)			Relative intensity (I)		
	Peak 1	Peak 2	Peak 3	Peak 1	Peak 2	Peak 3	Peak 1	Peak 2	Peak 3
1	7.04	7.11	7.11	-90.00	-150.15	150.15	322.74	323.43	321.52
2	8.44	5.40	7.52	-105.68	-152.33	167.85	328.46	306.87	317.96
3	6.58	7.14	7.57	-147.36	158.20	90.87	426.08	280.39	189.61
4	4.94	7.94	10.63	113.27	133.07	-92.44	570.25	127.11	160.17

effectiveness of the developed model in identifying incident parameters.

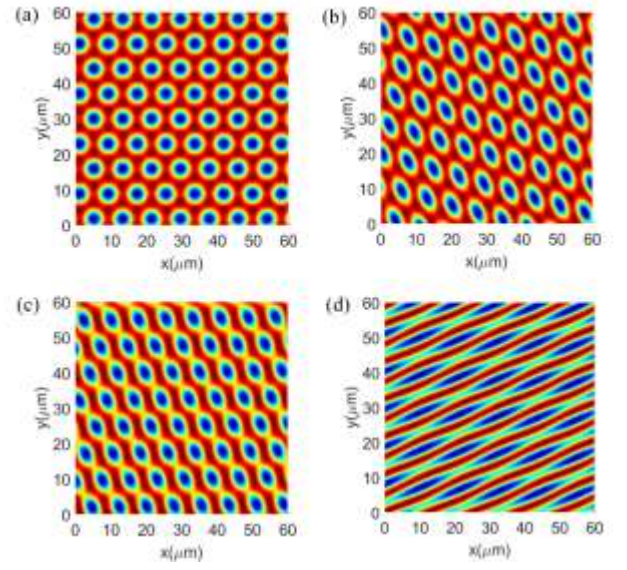


Fig. 2 Simulated results of three-beam laser interference patterns. (a)-(d) Simulated patterns corresponding to Nos. 1-4.

Table 3 Calculated incident parameters ($^\circ$)

No.	θ_1	θ_2	θ_3	ϕ_1	ϕ_2	ϕ_3
1	4.95	5.04	4.96	-0.2	119.7	239.7
2	7.08	1.98	6.01	0.1	120.1	240.7
3	4.99	5.01	5.08	9.5	127.0	235.3
4	5.26	7.41	3.93	307.9	102.9	23.9

4. Experimental validation and discussion

A three-beam interference system was built up using a Q-switched high-power Nd:YAG laser source with a wavelength of 1064 nm, pulse duration of 7 ns, frequency of 10 Hz, and Gaussian beam of 6 mm in diameter. Fig. 3(a) is a photograph of the laser interference lithography system and Fig. 3(b) shows the schematic diagram of the set-up. In the diagram, HR represents a high reflective mirror, BS represents a beam splitter, P and Q are polarizers and quarter-wave plates respectively. The laser source was split into three laser beams by two beam splitters. The intensity of each laser beam was adjusted by changing the

angles between Q and P. In this experiment, the intensity of each laser beam was set at 30 mJ/cm^2 for every pulse (monitored by a Coherent LabMax-TOP laser power and energy meter). Finally the three laser beams were focused onto the same point on the sample substrate. All the incident angles were set as 4° and the azimuth angles were 0° , 120° and 240° . The polarization modes were all TE. A polished silicon wafer was chosen as the sample substrate. The silicon wafer was cut and washed with ethanol and deionized water in an ultrasonic bath, and dried with nitrogen. The sample substrates were exposed for 1s (300 mJ/cm^2), 2s (600 mJ/cm^2) and 3s (900 mJ/cm^2), respectively. After fabrication, the samples were measured with a Bruker Contour GT 3D optical profiler, it is a white-light interferometric microscope with a lateral resolution of $0.26\text{ }\mu\text{m}$. The objective used in the experiment was a 50x lens. The camera in the profiler was a 640×480 standard monochrome camera.

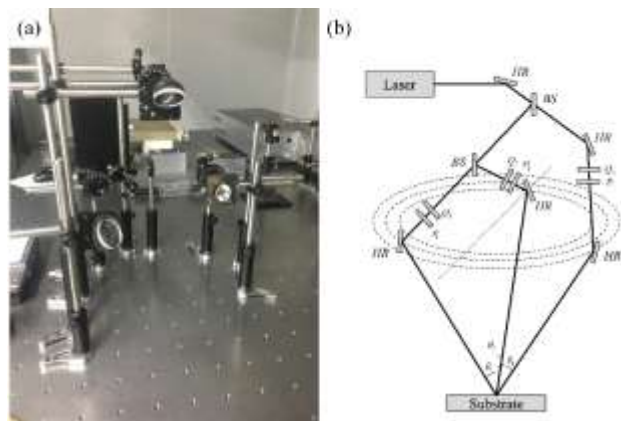


Fig. 3 Photograph (a) and schematic diagram (b) of the three-beam laser interference system

The theoretical pattern of interference intensity is shown in Fig. 4(a). The periods of the interference components were all calculated to be $8.81\text{ }\mu\text{m}$. The orientations of the interferences were 30° , 150° , and 270° . The intensities of the components were exactly all identical. Compared with the simulated laser intensity, the structures on sample surfaces shown in Figs. 4(c), (e), and (g) (exposed for 1s, 2s and 3s, respectively) have larger periods. This is mainly caused by misalignment of the incident parameters. The APSD images of the sample surfaces were generated and shown in Figs. 4(d), (f) and (h). The peaks in the circles represent the three interference components for each sample surface. After extracting the position and amplitude of the peaks the incident angle and azimuth angle of each incident laser beam was calculated and listed in Table 4. It can be observed from the results that the incident angles of laser beam Nos.1 and 2 in the three samples were all close to 3.5° , while the incident angles of laser beam No. 3 were around 3.8° . The calculated azimuth angles of the incident laser beams in the three samples also showed high consistency. For

incident beams the average incident angles were calculated as 3.45° , the azimuth angles were calculated as 3.58° , 3.77° , and 0.32° , 120.38° , and 239.31° . The simulated interference pattern using the calculated result is shown in Fig. 4(b), in which the period and distribution of the pattern is in good agreement with the experimental result.

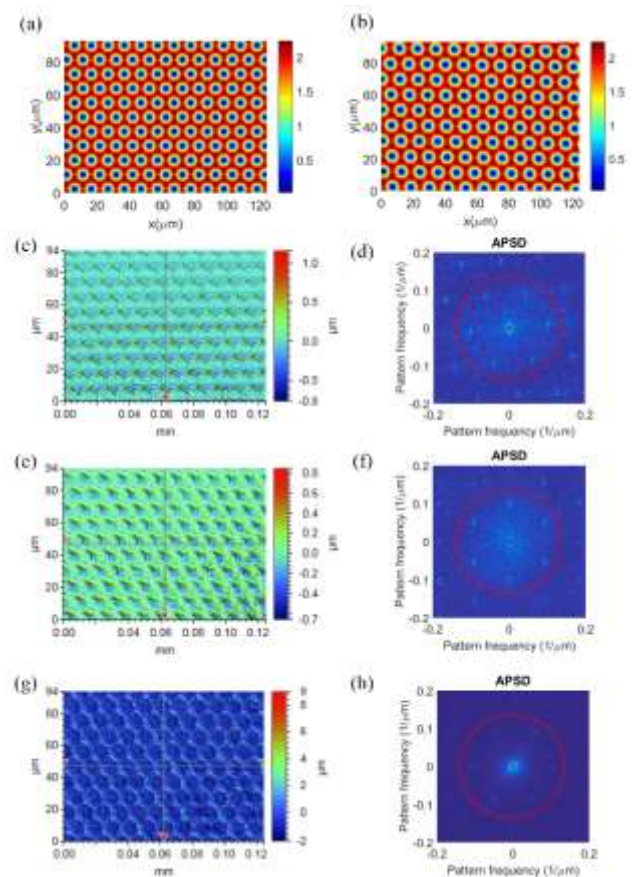


Fig. 4 Simulated interference intensity pattern, experimental topographies and their APSD images. (a) Simulated theoretical pattern. (b) Simulated pattern using calculated parameters. (c)–(h) 3D topographies and APSD images of sample Nos. 1-3.

5. Conclusion

An algorithm for incident parameter identification of laser interference beams has been established. The methodology for extracting interference fringes from complicated multi-beam interference patterns based on the APSD function has been developed. The algorithm could be used to calculate the errors in the interference system set-up that may lead to significant pattern deformations. The developed algorithm has been validated through both computational simulations and experimental testing. The 3D patterns fabricated by three-beam interferences on the silicon wafer samples were measured by optical profiler and then compared to the computational calculations based on the developed model. The good agreement between the results indicates that the proposed algorithm is effective for the incident parameter identification.

Table 4 Calculated incident parameters

Sample No.	Exposure time (s)	Peak No.	Period ($P / \mu\text{m}$)	Orientation ($\gamma / ^\circ$)	Relative intensity (I)	Beam No.	Incident angle ($\theta / ^\circ$)	Azimuth angle ($\phi / ^\circ$)
1	1	1	9.57	-174.51	2.44	1	3.51	0.14
		2	9.72	127.09	2.44	2	3.63	119.86
		3	10.06	-115.02	2.41	3	3.73	240.00
2	2	1	9.55	151.48	8.39	1	3.51	0.40
		2	9.55	-151.48	8.69	2	3.55	119.99
		3	10.00	-90.00	8.39	3	3.84	239.61
3	3	1	9.84	-122.12	1.32	1	3.35	0.42
		2	10.15	119.17	1.27	2	3.56	121.25
		3	9.80	180.00	1.13	3	3.73	238.32

Acknowledgement

This work was supported by Program of International S&T Cooperation (2016YFE0112100), National Key R&D Program of China (No. 2017YFB1104700) and EU H2020 Project (MNR4SCell 734174). The authors appreciate the technical support from Professor Zuobin Wang in Changchun University of Science and Technology (CUST).

References

- [1] A. Y. Vorobyev and C. Guo, *Laser & Photonics Reviews* 7(3), 385-407 (2013).
- [2] V. Lang, T. Roch and A. F. Lasagni, *Advanced Engineering Materials* 18(8), 1342-1348 (2016).
- [3] C. He, K. Vannahme and A. Gillner, *Journal of Laser Micro/Nanoengineering* 14(1), 95-99 (2019).
- [4] Y. Hu, Z. Wang, Z. Weng, M. Yu and D. Wang, *Applied optics* 55(12), 3226-3232 (2016).
- [5] D. G. Kim, S. H. Kim, H. C. Ki, T. U. Kim, J. C. Shin and Y. W. Choi, *Optical and Quantum Electronics* 50(9), 347 (2018).
- [6] B. H. Luo, P. W. Shum, Z. F. Zhou and K. Y. Li, *Surface and Coatings Technology* 204(8), 1180-1185 (2010).
- [7] J. Wang, L. Gao, Y. Li and B. Liu, *Lasers in medical science* 32(1), 221-227 (2017).
- [8] J. W. Leem, S. Kim, S. H. Lee, J. A. Rogers, E. Kim and J. S. Yu, *Advanced Energy Materials* 4(8), 1301315 (2014).
- [9] M. Gedvilas, S. Indrišiūnas, B. Voisiat, E. Stankevičius, A. Selskis and G. Račiukaitis, *Physical Chemistry Chemical Physics* 20(17), 12166-12174 (2018).
- [10] J. Xu, Z. Wang, Z. Zhang, D. Wang and Z. Weng, *Journal of Applied Physics* 115(20), 203101 (2014).
- [11] L. Hao, Y. Kai, L. Yan-Yan, G. Dong, Z. Qiu-Ling and W. Xia, *ACTA PHYSICA SINICA* 66(21), 217801 (2017).
- [12] R. Guo, D. Yuan and S. Das, *Journal of micromechanics and microengineering* 21(1), 015010 (2010).
- [13] M. N. Liu, L. Wang, Y. H. Yu and A. W. Li, *Optical Materials Express* 7(7), 2208-2217 (2017).
- [14] X. Ning, Q. Meng, L. Li, Y. Han, D. Zhou, L. Cao, Z. Weng, R. Ding and Z. Wang, In *Manipulation, Manufacturing and Measurement on the Nanoscale (3M-NANO), 2017 IEEE International Conference on* (pp. 375-378), IEEE, (2017).
- [15] B. Voisiat, M. Gedvilas, S. Indrišiūnas and G. Račiukaitis, *Physics procedia* 12, 116-124 (2011).
- [16] M. Bieda, M. Siebold and A. F. Lasagni, *Applied Surface Science* 387, 175-182 (2016).
- [17] D. Yuan, R. Acharya and S. Das, *Applied Physics Letters* 103(22), 223101 (2013).
- [18] D. Wang, Z. Wang, Z. Zhang, Y. Yue, D. Li and C. Maple, *Applied physics letters* 102(8), 081903 (2013).
- [19] T. Tavera, N. Pérez, A. Rodríguez, P. Yurrita, S. M. Olaizola and E. Castano, *Applied surface science* 258(3), 1175-1180 (2011).
- [20] D. Wang, Z. Wang, Z. Zhang, Y. Yue, D. Li, R. Qiu and C. Maple, *Journal of Applied Physics* 115(23), 233101 (2014).
- [21] C. Tan, C. S. Peng, V. N. Petryakov, Y. K. Verevkin, J. Zhang, Z. Wang, S. M. Olaizola, T. Berthou, S. Tisserand and M. Pessa, *New Journal of physics* 10(2), 023023 (2008).
- [22] M. Yu, C. Tan, Z. Wang, L. Zhao and W. Li, In *Manipulation, Manufacturing and Measurement on the Nanoscale (3M-NANO), 2013 International Conference on* (pp. 74-77), IEEE, (2013).
- [23] Y. Nakata and N. Miyanaga, *Applied Physics A* 98(2), 401 (2010).